

# Comparative Analysis and Ensemble Enhancement of Leading CNN Architectures for Breast Cancer Classification

Gary Murphy, Raghubir Singh, *Member, IEEE*

**Abstract**—This study introduces a novel and accurate approach to breast cancer classification using histopathology images. It systematically compares leading Convolutional Neural Network (CNN) models across varying image datasets, identifies their optimal hyperparameters, and ranks them based on classification efficacy. To maximize classification accuracy for each model we explore, the effects of data augmentation, alternative fully-connected layers, model training hyperparameter settings, and, the advantages of retraining models versus using pre-trained weights. Our methodology includes several original concepts, including serializing generated datasets to ensure consistent data conditions across training runs and significantly reducing training duration. Combined with automated curation of results, this enabled the exploration of over 2,000 training permutations - such a comprehensive comparison is as yet unprecedented. Our findings establish the settings required to achieve exceptional classification accuracy for standalone CNN models and rank them by model efficacy. Based on these results, we propose ensemble architectures that stack three high-performing standalone CNN models together with diverse classifiers, resulting in improved classification accuracy. The ability to systematically run so many model permutations to get the best outcomes gives rise to very high quality results, including 99.75% for BreakHis x40 and BreakHis x200 and 95.18% for the Bach datasets when split into train, validation and test datasets. The Bach Online blind challenge, yielded 89% using this approach. Whilst this study is based on breast cancer histopathology image datasets, the methodology is equally applicable to other medical image datasets.

**Index Terms**—Breast cancer, Convolutional Neural Networks Comparison, Dataset serialization, Ensemble architectures, Reduced Training Duration

## I. INTRODUCTION

### A. Breast Cancer

Breast cancer globally is the most common form of cancer in women and the second most common form of any cancer [17]. It is estimated that there are 2.3m cases diagnosed globally each year [1]. It is also the leading cause of female death by cancer – 684,996 in 2020. [1]. It remains a significant global health challenge, with its impact and mortality partly mitigated by advances in screening and treatment, particularly in developed countries.

Widespread adoption of screening programmes is seen as a critical step in lowering death rates in Breast Cancer in less

developed countries and as such is a key goal of the Breast Health Global Initiative [34]. AI assisted Breast Cancer screening, offers potential in both developed and under-developed countries not just by improving accuracy, but in lowering the cost of detection through its efficiency.

This study focuses on the use of CNNs for breast cancer detection and classification based on histopathology image datasets. Through direct model comparison on different image datasets it seeks to determine which architecture(s) and which settings are most suitable for this task.

### B. CNNs

CNNs have revolutionised computer vision and classification, taking inspiration from the neural architecture of the visual cortex in mammals' vision [3]. Fukushima's ground-breaking neocognitron [2] together with early innovators such as LeCun [4] set the foundations for the evolution of CNNs into the powerful models available today.

Since the inception of the ILSVRC [6], and the pioneering breakthrough in accuracy of AlexNet [7], illustrated in Fig. 1, also notable for exploiting GPUs for processing, increasing computer resources have permitted creation of deeper networks, such as the VGG models, VGG16 and VGG19 [8].

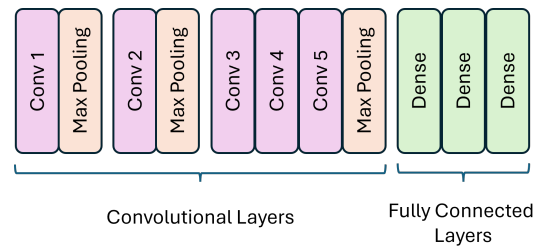


Fig. 1. Basic block architecture of AlexNet [7]

Subsequently CNNs evolved towards architectures prioritising efficiency and dealing with the problems surrounding ever deeper networks, such as vanishing gradients.

A raft of innovative CNN architectures have resulted, such as Inception [9], ResNets [10] and other architectures that aimed to be more efficient, rather than just adding more and more layers. These include DenseNets [12], Xception [18], NASNets [14], MobileNetV2 [13] and EfficientNets [11]. Variants of all these CNN models are fully optimised and evenly tested and compared against each other for breast cancer classification of histopathology images in this study.

This research did not receive any specific grant from funding agencies in the public, commercial, or not-for-profit sectors.

G. Murphy, and R. Singh are with the University of Bath, Claverton Down, Bath, BA2 7AY, United Kingdom (e-mail:gpjm20@bath.ac.uk; rs3022@bath.ac.uk).

These later, more complex models have many more layers than the relatively simple AlexNet architecture of 5 Convolutional and 3 Fully Connected (or Dense) layers. As an example the architecture of ResNet50 shown in Fig. 2 provides an at-a-glance comparison with that of AlexNet.

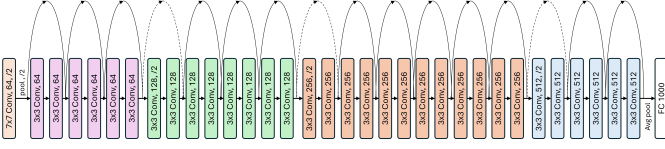


Fig. 2. ResNet50 Simplified Block Architecture showing the 34 layers with learnable parameters. The arced lines show the 'shortcuts' introduced in the model to enable its residual capability. Redrawn and transposed from vertical to horizontal [10].

### C. CNNs in Breast Cancer Classification

In general, research using AI for breast cancer detection and classification based on histopathology images has been conducted as a series of isolated studies arising from specific, singular datasets. These include the Bach challenge [16], and the BreakHis image dataset [21].

## II. RELATED WORKS

### A. Table of Related Works

Table. I summarises related work on the two datasets tested in this study. It is not an exhaustive list, but it represents some of the more well known studies.

Author(s)	Year	Models	Data Set	Highest Accuracy
Spanhol et al [23]	2015	AlexNet	BreakHis x40	90%
Bayramoglu et al [30]	2016	Bespoke	BreakHis x40	89%
Nawaz et al [26]	2018	DenseNet	BreakHis x100	97.86%
Deniz et al [27]	2018	AlexNet + VGG16 + SVM	BreakHis	91.87%
Vidyathi et al [29]	2019	LeNet-5 + CLAHE + Watershed	BreakHis	90%
Alom et al [32]	2019	IRRCNN	BreakHisx100	97.59%
Das et al [25]	2020	Bespoke CNN + MIL	BreakHisx200	93.04%
Mewanda et al [28]	2020	IRRCNN	BreakHis	97.58%
Wang et al [24]	2018	VGG16, SVM	Bach2018	81.25%
Wang et al [24]	2018	VGG16 (only)	Bach2018	92.50%
Rahklin et al [31]	2018	ResNet50, VGG16, InceptionV3	Bach2018	87.20%
Weiss et al [35]	2018	Xception, ResNet50 + VGG16 + LR	Bach2018	83%
Gour et al [22]	2020	ResHist (ResNet based)	Bach2018	92.62%

TABLE I  
TABULATED RELATED WORKS SUMMARY

### B. Existing comparison of works

M. Zhu et al's 2023 paper [20] is notable and commendable as a resource for comparing existing CNN research in breast cancer classification.

However, the insular nature of the underlying studies makes comparing the relative efficacy and strengths and weaknesses of the CNN models themselves challenging. Superior performance across different studies is likely influenced more by variations in augmentation techniques, other pre-processing steps, and the innovations within the individual projects, rather than the inherent performance of the CNN models. Although the paper provides insight into the best results, it does not (and cannot) clearly identify the best models.

In addition, general research and Zhu et al.'s paper [20] highlight the absence of some contemporary CNN models that are likely well-suited for the fine-grained analysis and feature detection required in histopathology images. Notable examples include EfficientNets [11], NASNets [14], and MobileNetV2 [13].

As can be seen from Table. I, there have been studies using ensemble models but these are in the minority. Deniz et al [27] and Weiss et al [35] both employing combinations of CNN models with traditional machine learning classifiers - SVM (Support Vector Machine) and LR (Logistic Regression) respectively. These are significant as they are conceptually similar to the ensemble models developed as part of this study. There are some studies that have considered multiple datasets, such as Mewada et al's study [28], but in general most studies have only considered a single dataset and, if competition based, focused solely on overall classification accuracy.

## III. AIMS AND CONTRIBUTIONS

This study seeks to determine the best CNN models and their optimum settings to achieve high quality results. Furthermore, to ascertain whether novel combinations of these models could provide even greater efficacy in breast cancer classification on histopathology based images. It aims to achieve this by:

- **CNN Model Comparison.** Systematically comparing a range of leading standalone CNN architectures with a goal of identifying which are most suited for breast cancer classification on histopathology images. Such a detailed comparison has not yet been undertaken. This includes establishing the optimal hyperparameters, the impact of varying the complexity of fully connected layers prior to classification, and establishing the advantages and disadvantages of using existing model weights.
- **Augmentation Insights.** Evaluating the effect of various augmentation techniques and hyperparameter settings.
- **Innovative and accurate Ensemble Architectures.** Combining high performing CNN models with complementary architectural features with diverse classifiers to construct innovative ensemble architectures, with a goal of achieving higher accuracy than their standalone counterparts.
- **Methodology.** Developing a framework and methodology for testing and comparing these models under standardised conditions. This includes the novel practice of pre-generating datasets to significantly expedite batched model runs and ensure identical conditions for model comparison. This, combined with automation of results across multiple runs for rapid analysis and comparison, facilitated the testing of a large number of permutations, in excess of 2000 model runs, to determine the best settings and thus highest quality results.

## IV. DATASETS TESTED

This study focuses on the following two datasets. One being a more simple binary classification challenge, binary or malignant, the other being a multi classification challenge, benign, insitu, invasive or normal.

### A. BreakHis Dataset

The BreakHis dataset of malignant and benign images released by F. A. Spanhol et al in 2015 [21], published 7909 breast cancer histopathology images of varying magnifications (x40, x100, x200, x400). The BreakHis dataset were labelled in a binary fashion: malignant or benign. In general the class distribution between malignant and benign images is not even and is in the approximate ratio of 2.2:1, apart from the x400 magnification dataset which is in the ratio 2.1:1.

### B. Bach 2018 Dataset

The Bach (BreAst Cancer Histology) dataset released as part of the Bach grand challenge on breast cancer histology images by G. Aresta et al [16] in 2018. This was a smaller dataset, 400 images, spread evenly across 4 classifications: Normal, Benign, InSitu and Invasive. The findings from the challenge can be found published in the ICIAR 2018 conference proceedings in Springer, [33].

The challenge also provides a separate testing dataset of 100 images. Whilst these cannot be utilised in the wider study, it is possible to use trained models and settings to predict class labels for these images and submit them for a "blind" marking. This was undertaken in this study. The results are discussed in section VIII-D.

## V. MODELS TESTED

### A. Standalone Models

The following standalone CNN models were evaluated:

- VGG16, VGG19 [8]
- InceptionV3 [19]
- ResNet50, ResNet152 [10]
- DenseNet121 [12]
- Xception [18]
- NASNetMobile [14]
- MobileNetV2 [13]
- EfficientNetV2B1 [11]
- AlexNet [7]
- LeNet-5 [5]
- Bespoke (Section V-B)

AlexNet and LeNet were tested for historical purposes to demonstrate CNN evolution. In addition to industry standard models, a Bespoke Model was implemented as outlined in section V-B.

### B. Bespoke Model Architecture

In addition to using established CNN models from keras.applications, it was valuable and informative to develop a bespoke model, designed specifically for the fine grained feature extraction challenges required by medical image classification. Whilst simpler than more complex architectures such as InceptionV3 [19] or ResNet50 [10] with which it was unlikely to compete, this model, designed for efficiency and accuracy, achieved commendable performance, even outscoring more complex models such as the VGG models [8].

The bespoke CNN model architecture is illustrated in Fig. 3:

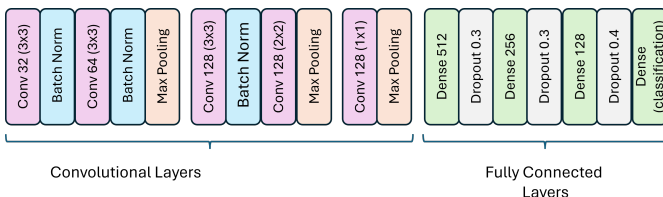


Fig. 3. Bespoke CNN Model Architecture

### C. Ensemble Architectures

Based on the principle of leveraging diversity to enhance model robustness and accuracy, we subsequently integrate CNN models with distinct architectural advantages to harness their complementary strengths into ensemble architectures combined with diverse classifiers. The following CNN models are stacked together:

- 1) DenseNet121 [12] + InceptionV3 [19] + NASNetMobile [14]
- 2) EfficientNetV2B1 [11] + InceptionV3 [19] + ResNet50 [10]
- 3) DenseNet121 [12] + InceptionV3 [19] + ResNet50 [10]
- 4) DenseNet121 [12] + InceptionV3 [19] + MobileNetV2 [13]

The stacked features from each of the three combined CNNs are married to one the following 4 classifiers, giving rise to 4 ensemble architectures per Tri-CNN model combination. The numbering in this section gives rise to the shorthand notation for the Ensembles. For example, Ensemble 1a is DenseNet121, InceptionV3, NASNetMobile + LR which is further abbreviated in some of the densely populated tables to Ens 1a.

- a) **Logistic Regression - LR** models the probability that an observation belongs to a specific class. One might expect strong performance on the BreakHis datasets, which involve binary classifications. However, LR's effectiveness can be sensitive to class distribution [40], and with a ratio of approximately 2.2:1 for malignant to benign images, this imbalance could reduce its accuracy.

Despite being a multi-classification problem, the Bach dataset, with its evenly distributed classes, demonstrates the efficacy of LR when class distribution is balanced. Although scikit-learn offers a 'multi\_class='multinomial'' setting, the simpler 'ovr' (one-vs-rest) setting was favoured by GridSearch over multinomial for both BreakHis and Bach datasets. Thus, the model operated as a series of binary logistic regressions. GridSearch also determined that LR would employ the LBFGS solver for all datasets, a Limited-memory Broyden-Fletcher-Goldfarb-Shanno algorithm, which is effective for handling large datasets. For a binary classification problem ('ovr' mode), where the response variable  $Y$  takes values in  $\{1, 2\}$ , given predictor variables  $\mathbf{x} = (x_1, x_2, \dots, x_p)^T$ , LR models the log-odds of the probabilities as follows [38]:

$$\log \left( \frac{P(Y = 1 | \mathbf{x})}{P(Y = 2 | \mathbf{x})} \right) = \beta_0 + \beta^T \mathbf{x} \quad (1)$$

where:

- $\beta_0$  is the intercept term.
- $\beta = (\beta_1, \beta_2, \dots, \beta_p)^T$  are the coefficients corresponding to each predictor variable, where  $p$  represents the number of features (or predictor variables) in the model.

From the log-odds, the probabilities can be derived as:

$$P(Y = 1 | \mathbf{x}) = \frac{\exp(\beta_0 + \beta^T \mathbf{x})}{1 + \exp(\beta_0 + \beta^T \mathbf{x})} \quad (2)$$

Given that  $P(Y = 2 | \mathbf{x}) = 1 - P(Y = 1 | \mathbf{x})$ , we have:

$$P(Y = 2 | \mathbf{x}) = \frac{1}{1 + \exp(\beta_0 + \beta^T \mathbf{x})} \quad (3)$$

Note: The equations provided here represent a simplified case of logistic regression, specifically for binary classification or when the multi\_class setting is set to 'ovr' (one-vs-rest).

- b) **Support Vector Classification - SVC** is designed to find the optimal hyperplane that maximizes the margin between different classes. It is capable of non-linear classification, which, achieved through the "kernel trick," enables it to discern complex patterns found in histopathology images [36]. The kernel trick uses kernel functions to implicitly project data into a higher-dimensional space. This approach relies on calculating the dot product from the input vectors to determine the similarity between classes, allowing the algorithm to find an optimal

separating hyperplane in this new feature space without directly computing the transformation.

SVC excels at higher magnifications, achieving the highest accuracy for any ensemble architecture in the BreakHis x400, and combined BreakHis datasets. It potentially handles the intricate details and textures present at higher magnifications more effectively than at lower magnifications.

Formulation of the hyperplane and margin, as defined by Cortes and Vapnik [36], can be shown as:

$$\min_{\mathbf{w}, b} \frac{1}{2} \|\mathbf{w}\|^2 + CF \left( \sum_{i=1}^l \xi_i \right) \quad (4)$$

subject to:  $y_i(\mathbf{w}^T \phi(\mathbf{x}_i) + b) \geq 1 - \xi_i$ ,  $\xi_i \geq 0$  [41]

Where:

- $\mathbf{w}$  is the normal vector to the hyperplane.
- $b$  is the bias term in the decision function.
- $C$ , a constant, is the regularization parameter that controls the trade-off between achieving a low training error and minimizing model complexity for better generalization.
- $\xi_i$  are the slack variables that allow for misclassification; larger values permit more violations of the margin.  $\xi_i = 0$  for correctly classified points that lie outside or on the margin;  $\xi_i > 0$  for misclassified points (inside the margin).
- $\phi(\mathbf{x}_i)$  maps  $\mathbf{x}_i$  to a higher-dimensional space, enabling the capture of non-linear patterns through the kernel trick. For a linear kernel, the decision function simplifies to  $\mathbf{w}^T \mathbf{x}_i + b \geq 1 - \xi_i$ .
- $F(u)$  is a monotonic convex function applied to the slack variables, designed to penalize margin violations. This function can vary; for example, a linear function  $F(\xi) = \xi$  (as in the standard SVC formulation as introduced by Cortes and Vapnik [36]) simply sums the violations, whereas a quadratic function  $F(\xi) = \xi^2$  penalizes larger violations more heavily. The choice of  $F$  affects the SVC's tolerance for errors and its generalization capabilities.

A key strength of SVC is its ability to select differing kernels to optimise its classification efficacy depending on dataset. The kernel is selected as part of a grid search process using Grid-SearchCV. For each dataset run, the regularization parameter, kernel type, kernel coefficient and degree of polynomial kernel (for the poly kernel) were selected depending on the validation dataset. The Regularization parameter boundaries were pre-explored to identify the best range, in order to limit permutations and thus impact on computer resources. Depending on which provides optimum classification efficacy, in our implementation SVC can act as a simple linear classifier or employ more complex decision boundaries using the 'rbf' or 'poly' kernels.

- c) **Random Forest - RF** is an ensemble learning method renowned for its robustness and accuracy across various applications. RF constructs multiple decision trees during training and outputs the class that is the mode of the classes predicted by individual trees. This method effectively reduces overfitting and enhances prediction accuracy, making it particularly suitable for complex classification tasks such as those found in histopathology images. [39]

RF employs the principles of bootstrap aggregation, known as bagging, to improve model stability and accuracy. Each tree in the forest is trained on a random bootstrap sample of the data, which means each tree sees a slightly different subset of the data. This process helps in reducing variance and avoiding overfitting. Additionally, RF utilizes the random subspace method, where each tree is not only trained on a random sample of data instances but also considers a random subset of features when making decisions. This feature randomness introduces further diversity among the trees in the forest, thereby enhancing the ensemble's ability to generalize across different datasets and reducing the likelihood of overfitting to noise present in the training data.

These characteristics make RF a powerful tool for handling datasets with complex structures and high-dimensional feature spaces, as to be found in histopathology image datasets. This is borne out in the results Table. III, which shows RF based ensembles at the top of the leaderboard.

- d) **Light Gradient Boosted Machine - LGBM** [37] is a powerful boosting algorithm that combines multiple weak classifiers (typically shallow decision trees) to form a strong predictive model. Its ability to handle imbalanced data effectively should make it particularly suitable for the BreakHis datasets, which have an imbalanced class distribution. LGBM's weak learners incrementally correct errors from previous iterations, enabling the model to learn complex patterns in the data - as required for fine-grained feature detection in histopathology images, such as breast cancer classification.

It seemed sage to employ a boosting algorithm and LGBM is chosen over XGBoost due to its lightweight nature and efficient performance. Unlike other boosting algorithms that grow trees level-wise, LGBM grows trees leaf-wise, which results in greater loss reduction and faster convergence. This leaf-wise approach can lead to better performance, especially on large datasets. In addition it required far less computing resources than XGBoost, which proved problematic to implement.

The update rule used by LGBM can be understood as a specific implementation of the general principles of boosting, which is a type of Forward Stagewise Additive Modelling [38]. (Note: As mentioned, LGBM distinguishes itself as a leaf-wise boosting algorithm, setting it apart from others such as XGBoost, which typically use level-wise growth.)

In each stage of the boosting process, LGBM aims to minimize the residual errors from the previous model iteration by adding a new weak learner  $h_m(x)$ . The model is updated iteratively using the formula:

$$F_m(x) = F_{m-1}(x) + \gamma_m h_m(x), \quad (5)$$

where:

- $F_{m-1}(x)$  is the model built up to the  $(m-1)$ th iteration.
- $h_m(x)$  is the new weak learner (typically a decision tree) added at iteration  $m$ .
- $\gamma_m$  is the learning rate, controlling the contribution of  $h_m(x)$  to the overall model.

## VI. RESEARCH METHODOLOGY

### A. Outline Concepts

- **Data Pre-processing:** Ensuring the images are in the required format (3 channel x 8 bits/channel), images randomly split into train (60%), validation (20%) and test (20%) and the directory structure reflects the image labels. Post splitting the datasets, a programmatic check to ensure there is no data leakage is initiated.
- **Augmentation:** Pre-Training - Generating augmented images to supplement training datasets.  
During Training - Comparing static augmentation (serializing datasets) with on-the-fly/dynamic augmentation.
- **Dataset Pre-generation:** Serializing datasets to numpy files to ensure identical conditions for each CNN model and to expedite training. See Section VI-E.
- **Dynamic Hyperparameters:** Enable runtime adjustment of hyperparameters for flexible experimentation, in addition to flags that, for example, control whether to use pre-existing weights, or to adopt fine-grained filtering by employing more fully connected layers (see section VI-G).
- **Efficient Training:** Use parameterised callbacks for early stopping, learning rate reduction on loss plateau, and saving the best model state when validation accuracy improves.
- **Novel ensemble architectures:** Creating ensemble models by combining high performing CNNs exhibiting complementary



architectures and diverse classifiers, based on insights from the CNN model comparison.

- **Comprehensive Quality Metrics:** Establishing quality metrics including Accuracy, Precision, Recall, F1, and Specificity, both as overall aggregates and per class for multi-classification datasets.
- **Parameter & Quality Metrics Serialization:** Storing all parameters and hyperparameters of every CNN and ensemble run in JSON files, combined with quality metrics from testing, to facilitate automated results analysis.

The two test cases, standalone CNN models and ensemble models, resulted in two highly parameterized code harnesses. These, together with other aspects of the methodology above, are discussed in the following sections.

### B. End-to-end Architecture

Fig. 4 outlines a simplified block architecture depicting the various stages of the methodology for each image dataset. Starting from image pre-processing, augmentation and pre-generation and serialization of datasets; through to multiple CNN model iterations based on different models and settings; through to ensemble models and post-processing.

The end-to-end method is broken down into three algorithms.

- Algorithm 1: outlines how optimum hyperparameter and other settings are established.
- Algorithm 2: outlines how the main standalone CNN harness may be instantiated in batch mode.
- Algorithm 3: outlines how the ensemble processing is effected.

### C. Data Pre-processing

For both image datasets, for each class (labelled by way of its sub-directory structure) the datasets were split - training:validation:testing ratio of 60:20:20, using `train_test_split` from `sklearn.model_selection`. Pre-processing of each dataset was slightly different as set out below:

1) *Bach 2018 Grand Challenge:* The Bach datasets can be downloaded from zenodo [16]. The zip file `ICAR2018_BACH_Challenge` has quite a straight forward structure with a root directory of Photos followed by sub-directories for Benign, InSitu, Invasive and Normal. Each sub-directory containing TIFF files of size 2048 x 1536 pixels, with a bit depth of 48, each approximately 18Mb in size.

Pre-processing was straightforward. The images were converted to 24bit (8 bit x3 channel) PNG files, of the same resolution but less than a quarter of the size at approximately 4Mb each.

2) *BreakHis Datasets:* The BreakHis datasets can be downloaded following instructions in Spanhol et al's paper [21]. The folder root directory has two sub-directories: benign and malignant.

Beneath both the benign and malignant sub-directories is a further sub-directory called SOB. Under SOB are more detailed classifications on the type of tumour, followed by the magnification level, x40, x100, x200, x400 with each of these directories containing the image files as 700 x 460 pixel, 24 bit. The BreakHis images did not need pre-processing, the images were collated into a simpler directory structure of x40, x100, x200, x400 each with a sub-directory for benign and one for malignant, each holding the respective images.

### D. Augmentation

Augmentation of the training image datasets was an important technique, particularly for the Bach dataset, which contained only 60 images per class once split into train, val and test datasets. As a result, augmentation significantly impacted training efficacy.

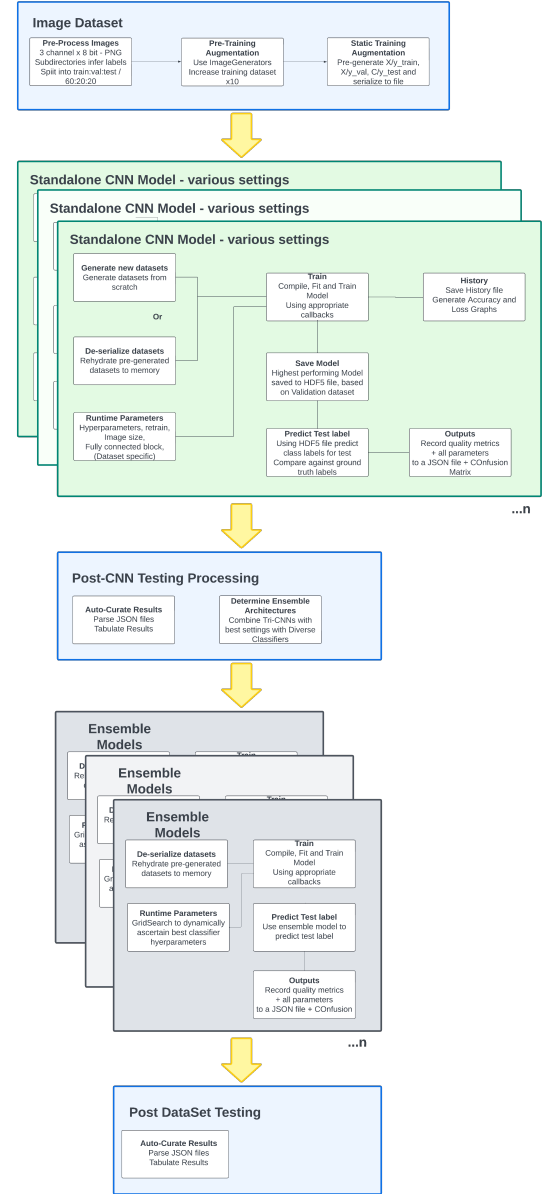


Fig. 4. End-to-end Architecture - Pre-processing, CNN models in a loop, Ensemble Models in a loop - inferences

1) *Pre-training: Augmentation To Enhance Training Datasets:* To increase the training dataset size, the `ImageDataGenerator` function from `keras.preprocessing.image` was used to generate and save additional augmented images from each source image.

Careful selection of augmentation parameters was necessary to avoid over-distortion of the images. For example, a typical 'fill\_mode' of 'nearest' could create tumor-like artifacts in the augmented images. Typical parameters found online were generally not suitable.

These parameters were used to generate 10 augmented images per original image in the training set.

2) *Augmentation During Training:* In-place data augmentation was employed during training using a slightly different set of parameters, but again chosen with care not to distort the image features.

For efficiency, all datasets generated during training were serialized to numpy files for reuse. This approach standardised `X_train` (as well as `X_val` and `X_test`) across multiple models and hyperparameter

---

**Algorithm 1:** Hyperparameter, Environment, and Runtime Settings

---

**Data:** Input Image Datasets  
**Result:** Best hyperparameters, Image Size, Fully Connected Block, Whether to retrain or use existing model weights, augmentation settings ->leading to pre-generated serialized datasets for training and optimised settings

```

for each Image Dataset do
  Pre-process input images - format; split into train, validation, test, with sub-directories inferring class labels;
  Establish best settings on non-augmented data;
  Perform electronic data leak test across directories;
  for each iteration establish the optimum settings for: Initial learning rate (LR); LR Decay; Patience for Early Stopping and Reduce LR on plateau; Input image size; Retrain every layer vs. use existing weights; Complex fully connected block vs. simple block; Batch Size; do
    Compare results, if increased accuracy and amend setting
  end
  Establish best pre-training augmentation generation settings using ImageDataGenerator;
  for each iteration do
    Rotation range, fill_mode, width/height_shift_range;
    Shear_range, zoom_range, horizontal/vertical_flip;
    Brightness_range;
  end
  Pre-generate training datasets using ImageDataGenerator and FlowFromDirectory, serialize to file;
end

```

---

settings, ensuring that each model was trained on exactly the same dataset.

Although serializing and reusing  $X_{train}$  potentially loses some of the benefit of on-the-fly augmentation, which dynamically introduces variability to reduce overfitting, it still provided an improvement over training with the original images alone. We termed this static-augmentation at training.

The outcomes of the augmentation approaches are detailed in section VIII-A.

#### E. Dataset Pre-generation

As discussed in the previous section the three datasets datasets, training, validation and testing were pre-generated and serialized to file. This approach ensured consistent data conditions and significantly expedited model training. It allowed for consistent comparisons across more than 2000 model runs.

#### F. CNN Model Harness

Central to the methodology and framework is the development of a runtime configurable harness that can accept the core CNN model, the input dataset, and various runtime and model hyperparameters.

---

**Algorithm 2:** Main Standalone Model Comparison

---

**Data:** Pre-Generated Image Datasets  
**Result:** Model training run ->runtime hyperparameters and results persisted to JSON file; Model persisted to HDF5 file

```

for each Image Dataset do
  for each model in {BespokeModel, AlexNet, LeNet-5, DenseNet121, InceptionV3, ResNet50, ResNet152, EfficientNetV2B1, NASNetMobile, MobileNetV2, Xception, VGG16, VGG19} do
    Deserialize datasets to memory;
    Invoke training harness;;
    Create directories;
    Create model;
    Add callbacks;
    if fine-grained filter set then
      Add complex fully-connected pre-classifier block;
    else
      Add simpler fully-connected pre-classifier block;
    end
    Compile and fit model to  $X_{train}, y_{train}$ , validating with  $X_{val}, y_{val}$ ;
    Save history file and create Accuracy and Loss by Epoch training graphs;
    Reload best saved model from HDF5 file;
    Predict class labels for  $X_{test}$ ;
    Compare predicted labels against ground truth labels ( $y_{test}$ );
    Generate Confusion matrix and quality metrics from TP, TN, FP, FN per class;
    Save all parameters and quality metrics per class to JSON file;
  end
end

```

---

The primary benefit of this function is that it allows for multiple calls to batch test multiple models in a loop with varying runtime parameters. The logic of the CNN model testing harness is outlined in Algorithm 2.

#### G. Coarse or Fine Grained - Fully-Connected Pre-Classification blocks

Each CNN model is loaded without the very topmost layer (the classification layer) and a uniform classification construct is added. The harness tests using a simple fully connected layer block or a more complex one, prior to classification, as determined by the fine\_grained hyperparameter.

The two variants are shown in Fig. 5. The fine-grained model was particularly effective for the Bach dataset [16], albeit less marked for the BreakHis binary classification datasets [21]. The impacts on the classification accuracy for the Bach dataset are detailed in Section VIII-C in Table. VII.

It should be noted than the additional dense layers add significantly to the number of trainable parameters in a CNN, and thus computational resources required. As such its use was not recommended or used for the BreakHis datasets. This underlines the importance of flexible settings that may vary per image dataset characteristics.

---

**Algorithm 3: Ensemble Model Processing**


---

**Data:** Pre-Generated Image Datasets

**Result:** Ensemble models, optimised parameters and results persisted to a JSON file

**for each Image Dataset do**

 Establish best models for Ensemble Architectures;  
 (Stack three CNN models with LR, SVC, RF,  
 LGBM classifiers, yielding 4 ensembles);

**for each set of 3 CNN models to form an ensemble do**

 Load the models from HDF5 files up to the  
 layer before classification (feature maps);  
 Deserialize the datasets to memory;  
 Create feature maps for train, val, and test for  
 each of the 3 CNN models;  
 Concatenate the feature maps from each of the  
 models for each dataset;

**for each of the 4 classifiers selected do**

 Establish best hyperparameters using  
 GridSearch on the Validation feature map;  
 Create the classifier using the best  
 hyperparameters;  
 Fit the classifier to the combined features  
 of the training feature map;  
 Predict class labels against test feature map;  
 Compare predicted labels against ground  
 truth labels ( $y_{test}$ );  
 Generate Confusion matrix and quality  
 metrics from TP, TN, FP, FN per class;  
 Save all parameters and quality metrics per  
 class to JSON file;

**end**
**end**
**end**


---

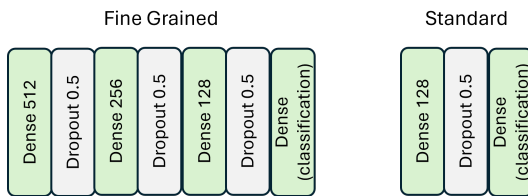


Fig. 5. Dense block classification variants

### H. Ensemble Model harness

Complementing the CNN harness is another harness for the ensemble architectures. This enables the injection of either 2 or 3 model files from the CNN training (HDF5 files) combined with the classifiers: Logistic Regression, Support Vector Classifier, Random Forest, Light Gradient Boosted Machine. The logic for the ensemble harness is outlined in Algorithm 3.

### I. Parameter and Quality Metrics Serialization - automated results analysis

The hyperparameters.json file created for a standalone CNN model run and Ensemble architecture run are similar. For the CNN model runs, the JSON file captures information concerning the dataset name, whether it was augmented, whether the fine grain filter was applied,

the model name and where the model file is saved; together with all the hyperparameter settings that were employed together with the results, i.e. the quality metrics, when the trained model is used to predict class labels against the test dataset. For the ensemble model runs, the specific CNN hyperparameter settings are Not Applicable, but instead the hyperparameters selected by the GridSearch process are saved to the JSON file. In every other detail the two types of JSON file are identical. This enabled automatic parsing of a range of model runs, CNN and ensemble, to facilitate rapid results analysis and cross-model comparisons.

## VII. RUN OUTPUTS

The challenge with over 2000 runs, is that it is not possible to present all the result outputs in a journal paper. The Results section, is thus very condensed and presented as a series of tables, giving various insights into models and settings efficacy in highly summarised form. In particular with so many dimensions to show, some of the key quality metrics are not shown in these summary tables.

More detailed tables show all the outputs for a single dataset, using optimal hyperparameter, augmentation and other runtime settings - both in terms of results, confusion matrices and quality metrics. This information is replicated many hundreds of times. Specific run details can be furnished upon request.

### A. Standalone CNN Batch test outputs

Each CNN model run training generates the following files:

- A graph showing Validation and Training Accuracy by Epoch.
- A graph showing Validation and Training Loss by Epoch.
- A ".h5" (HDF5) file holding the best model and its weights.
- A JSON file storing the hyperparameters used and the results from the run. The latter are created by loading the HDF5 file and using it to predict the results from the test dataset.
- A confusion matrix from the test dataset predictions.

1) *Single Run Outputs:* The following are outputs from the BreakHis x40 magnification with augmentation and for DenseNet121. Fig. 6 shows the Training and Validation Loss and Accuracy plots. Fig. 7 shows the resulting Confusion Matrix plotted when using the saved HDF5 model file to predict the classifications against the test dataset.

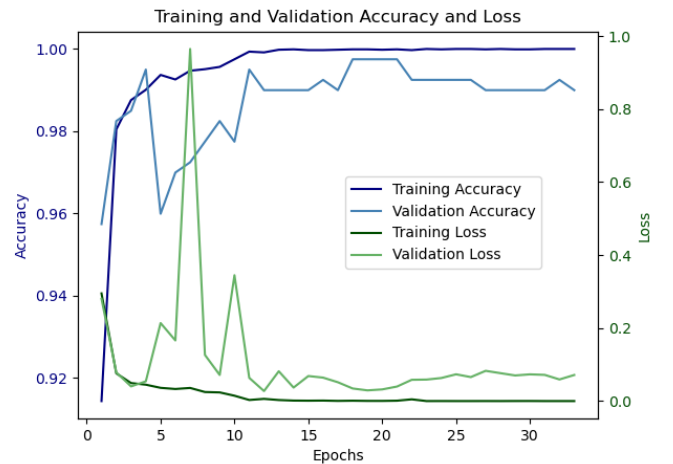


Fig. 6. Training &amp; Validation Accuracy for DenseNet121 on BreakHisx40

2) *Ensemble Run Outputs:* For an Ensemble Run, just the hyperparameters and Confusion Matrix are generated as the training graphs shown for standalone CNN models are not applicable. The model may also be saved as a pickle file.

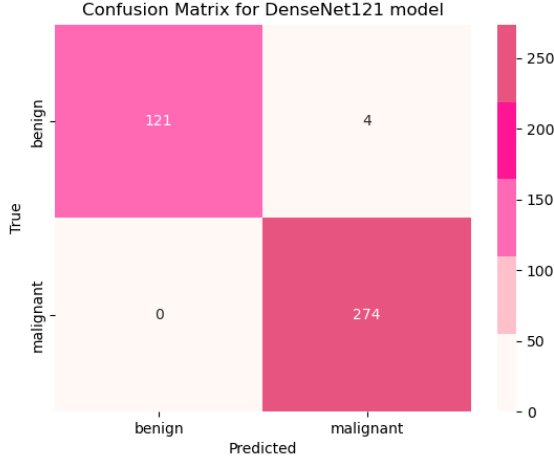


Fig. 7. Confusion Matrix for DenseNet121 on BreakHis x40

3) *Tabulated Results*: Having run all the CNN models and associated ensembles, we can then electronically auto-curate and tabulate the results, by parsing the directory structure and extracting the metrics from the hyperparameter.json files. Again, using the dataset BreakHis x40 in a fully retrained mode, using augmentation, an image size that preserved aspect ratio, and a range of hyperparameters, we get the results as shown in Table. II for both standalone and ensemble models.

Model	Acc	Recall	Prec'n	F1	Spec'ty
Ensemble 1d	99.75%	100.00%	99.64%	99.82%	99.20%
InceptionV3	99.50%	100.00%	99.28%	99.64%	98.40%
Ensemble 1b	99.50%	100.00%	99.28%	99.64%	98.40%
Ensemble 1c	99.25%	100.00%	98.92%	99.46%	97.60%
Ensemble 2a	99.25%	100.00%	98.92%	99.46%	97.60%
EfficientNetV2B1	99.25%	99.64%	99.27%	99.45%	98.40%
Ensemble 1a	99.25%	99.64%	99.27%	99.45%	98.40%
Ensemble 2b	99.25%	99.64%	99.27%	99.45%	98.40%
DenseNet121	99.00%	100.00%	98.56%	99.28%	96.80%
MobileNetV2	99.00%	99.64%	98.91%	99.27%	97.60%
NASNetMobile	99.00%	99.64%	98.91%	99.27%	97.60%
Ensemble 2d	99.00%	99.64%	98.91%	99.27%	97.60%
Ensemble 2c	99.00%	99.64%	98.91%	99.27%	97.60%
ResNet152	98.75%	100.00%	98.21%	99.10%	96.00%
Xception	98.75%	99.27%	98.91%	99.09%	97.60%
ResNet50	98.50%	100.00%	97.86%	98.92%	95.20%
Bespoke	92.23%	95.99%	92.93%	94.43%	84.00%
VGG16	90.73%	97.81%	89.63%	93.54%	75.20%
VGG19	90.23%	94.53%	91.52%	93.00%	80.80%
AlexNet	89.47%	97.08%	88.67%	92.68%	72.80%
LeNet	73.93%	97.81%	73.22%	83.75%	21.60%

TABLE II

RESULTS FOR BREAKHIS x40 MAGNIFICATION - AUGMENTED AND RETRAINED

Tables such as these were created for a wide range of settings across all models; using different augmentation strategies, different pre-classification fully connected blocks, different input image sizes and ratios, and a range of hyperparameter permutations such that the very best settings could be established by comparing these tables across settings. This was a key tenet of the method and framework.

## VIII. NUMERICAL RESULTS

Having ascertained the very best models and settings, using optimized hyperparameters, ignoring existing model weights, using image sizes that respected the aspect ratio of the source images,

augmentation and appropriate fully connected layers, it was clear that the differences between the top performing models was marginal and within the potential variation of a given training run. Despite using pre-generated datasets to ensure that images were processed in identical order and identical training augmentation, CNN model training can show slight variances between runs.

In order to more fully verify our results, we undertook more rigorous verification. This involved taking the best CNNs, with their associated optimised settings, for histopathology feature detection and cancer classification: DenseNet121 (DNet) [12], InceptionV3 (Incp'n) [19], ResNet50 (RNet50) and ResNet152 (RNet152) [10], Xception (Xcep'n) [18], NASNetMobile (NNMob) [14], MobileNetV2 (MNet) [13], EfficientNetV2B1 (ENet) [11], and testing each model on each dataset ten times each to form an average.

Ensembles 3(a,b,c,d) and 4(a,b,c,d) were also added at this time and each of the resulting 16 ensembles was tested a further 5 times, again to form an average. This verification phase of 8 CNN models and 16 ensemble models on 6 datasets, tested ten and five times respectively added an additional 960 runs. The averaged results, which show more scientific rigour are shown in Table. III. The weighted average (WtdAvg), by which it is ordered, makes each equal in significance to the average of the five BreakHis (BH) datasets.

Model	BHx40	BHx100	BHx200	BHx400	BHxAll	Bach	WtdAvg
Ens 4c	99.75%	98.90%	99.75%	97.92%	98.91%	95.18%	97.11%
Ens 3c	99.75%	98.90%	99.75%	97.81%	98.84%	95.18%	97.09%
Ens 3a	99.50%	99.52%	99.50%	97.81%	98.23%	95.18%	97.05%
Ens 2c	99.75%	98.47%	99.01%	98.03%	98.19%	95.18%	96.93%
Ens 3b	99.50%	99.28%	99.50%	97.81%	98.86%	94.58%	96.78%
Ens 1c	99.75%	99.14%	98.96%	98.08%	98.96%	94.58%	96.78%
Ens 1a	99.50%	99.28%	98.76%	98.08%	98.74%	94.58%	96.72%
Ens 2a	99.50%	98.56%	99.01%	97.26%	98.42%	94.58%	96.56%
Ens 4a	99.25%	98.56%	99.50%	97.53%	98.55%	93.37%	96.03%
DNet	98.79%	98.99%	99.11%	97.62%	98.29%	93.37%	95.97%
Ens 1b	99.75%	99.28%	99.26%	98.63%	98.86%	92.77%	95.96%
ENet	99.35%	98.37%	98.26%	96.33%	97.68%	93.86%	95.93%
Ens 2b	99.75%	98.80%	99.26%	98.36%	98.61%	92.77%	95.86%
Ens 4b	99.75%	99.04%	99.75%	97.81%	98.93%	92.17%	95.61%
Ens 2d	99.50%	96.64%	99.01%	97.81%	97.72%	92.77%	95.45%
Xcep'n	99.10%	98.61%	98.78%	96.85%	98.15%	92.53%	95.41%
Incp'n	98.78%	98.90%	98.83%	96.96%	97.49%	92.29%	95.24%
Ens 4d	99.50%	98.08%	99.50%	97.81%	98.61%	91.37%	95.03%
RNet152	97.99%	97.65%	97.30%	96.79%	96.17%	92.29%	94.73%
Ens 3d	99.50%	98.08%	99.01%	97.81%	98.61%	90.76%	94.68%
RNet50	98.30%	98.32%	98.44%	97.23%	96.36%	91.33%	94.53%
NNMob	98.75%	98.66%	98.04%	96.96%	98.37%	90.84%	94.50%
Ens 1d	99.50%	98.08%	96.77%	97.81%	98.55%	90.76%	94.50%
Mnet	99.22%	97.65%	97.42%	96.30%	97.91%	91.08%	94.39%

TABLE III

AVERAGED RESULTS LEADERBOARD AFTER EXTENSIVE TESTING

The marginal variations between runs, underlines the importance generally of multiple CNN runs to establish which are the best performing models and settings. The high accuracy obtained across all models is testament to the methodology of this study, and the performance of modern architected CNNs. Ensemble Architectures were found to slightly outperform their constituent CNN models.

The following sections detail the impacts of varying the training condition settings. Where direct comparisons are made, these are for single runs, and not based on the averages set out in Table. III.

### A. Impacts of Augmentation

This study conducted investigations on the use of augmentation as a means to boost training sample images, termed "Pre-Training Augmentation", and during training to avoid overfitting, termed "Augmentation During Training". The findings are discussed here:



1) *Pre-Training Augmentation:* Augmentation (section VI-D) was employed to generate 10 augmented images per original image in the training datasets. This significantly improved accuracy for all datasets, but the difference was particularly marked for the Bach dataset, including the blind challenge (see section VIII-D). The results, showing the highest accuracies achieved per dataset with and without pre-augmenting the training datasets are shown in Table. IV.

DataSet	No Augmentation	Augmentation
BreakHis x40	98.25%	99.75%
BreakHis x100	94.74%	99.04%
BreakHis x200	94.24%	99.50%
BreakHis x400	94.74%	97.81%
BreakHis combined	94.74%	98.29%
Bach	86.78%	94.58%
Bach blind test	80.00%	89.00%

TABLE IV

COMPARISON OF ACCURACY FOR CNN MODELS USING AUGMENTATION V NO AUGMENTATION

2) *Augmentation During Training:* The Training augmentation settings are purposely slightly different to the pre-generation augmentation settings. Training augmentation was employed in two different modes; Static and on-the-fly. The approaches and merits and drawbacks of each are discussed in section VI-D. The differences in performance between static and on-the-fly approaches is shown in Table. V.

DataSet	On-the-fly Augmentation	Static Augmentation
BreakHis x40	99.50%	99.75%
BreakHis x100	99.04%	99.04%
BreakHis x200	100.00%	99.50%
BreakHis x400	98.63%	97.81%
BreakHis combined	Not Tested	98.29%
Bach	Not Tested	94.58%
Bach blind test	87.00%	89.00%

TABLE V

CNN MODEL ACCURACY COMPARISON FOR ON-THE-FLY AUGMENTATION V STATIC AUGMENTATION

On-the-fly based augmentation is acknowledged to overall be superior, based on the theory of avoiding overfitting, but the benefits seen were minimal. In addition the Bach Online challenge [16], best results were achieved with static augmentation, see section VIII-D. The difference in training time however is vast so when considering multiple permutations static augmentation during training represents a good compromise and its approach is advocated in this study.

### B. Pre-loaded model weights v Re-training

The impact of fully retraining a model and ignoring the existing model weights is detailed in Table. VI. This underlines the relative uniqueness of histopathology images.

DataSet	Pre-loaded Weights	Re-trained
BreakHis x40	95.74%	99.75%
BreakHis x100	94.74%	99.04%
BreakHis x200	94.24%	99.50%
BreakHis x400	94.74%	97.81%
BreakHis combined	94.74%	98.29%
Bach	92.17%	94.58%

TABLE VI

A COMPARISON OF THE BEST ACCURACIES OBTAINED BY DATASET USING PRE-LOADED WEIGHTS AND RETRAINING FROM SCRATCH

### C. Impact of Fine Grained Fully Connected Block

The more complex fully-connected pre-classification block, termed fine grained, discussed in section VI-G, had a marked impact for the

multi-class Bach dataset, but not for the binary BreakHis dataset. It was found that the architecture of this block needed to be dataset specific, and should be a design consideration when working with other datasets.

Table. VII shows the best accuracies on the Bach dataset achieved with the Fine Grained and Coarse Grained pre-classification fully connected blocks respectively.

Model	Fine Grained	Course Grained
InceptionV3	93.98%	83.73%
DenseNet121	92.17%	88.55%
MobileNetV2	91.57%	84.34%
NASNetMobile	90.96%	83.13%
ResNet50	90.36%	62.65%
Xception	90.36%	88.55%
ResNet152	86.75%	62.05%
EfficientNetV2B1	86.14%	62.05%
VGG16	83.13%	82.53%
VGG19	82.53%	81.93%
Bespoke	81.93%	62.05%
AlexNet	79.52%	62.65%
LeNet	62.05%	62.65%

TABLE VII

COMPARISON OF ACCURACIES USING FINE GRAINED AND COARSE GRAINED CLASSIFICATION LAYERS ON STANDALONE CNN MODELS ON THE BACH DATASET [16].

### D. Bach Online blind challenge [16]

Whilst without labelling it isn't possible to use the Test images in the Bach Online Challenge to compare predicted labels against ground truth labels, it is possible to submit a CSV file with labels for the test file of 100 images for a blind marking to the Bach Grand Challenge [16]. This auto-marks the file and presents the results by way of a leaderboard: <https://iciar2018-challenge.grand-challenge.org/evaluation/part-a/leaderboard/>.

This provided an opportunity to benchmark the best CNN and Ensemble models on the competition site against all other entries in the competition to date. As at 27/07/2024 the leaderboard showed this paper's submission as 26th with 89% using Ensemble 3c. Subsequently Ensemble 1b also achieved this score. There are multiple duplicates by the same authors on the leaderboard, as such this study's submission was the 5th highest by author.

## IX. CONCLUSIONS

Systematic testing of multiple models with varying parameters and settings provided valuable insights into the relative efficacy of CNN and ensemble architectures in classifying breast cancer histopathology images, using the Bach [33] and BreakHis [21] benchmark datasets.

A novel aspect of the methodology concerned pre-generation of all data sets and serializing these to file. For the testing dataset, which had inline augmentation settings, this was termed static augmentation. This proved to be highly effective in expediting model training and ensuring consistent comparisons, forming a cornerstone of this study's methodology. The reduction in training duration enabled multiple environment and hyperparameter permutations to be tested in a timely manner.

A simpler innovation concerned the persistence of all the run and hyperparameter settings together with the results to JSON files, such that results could be automatically processed for rapid analysis.

Together these facilitated the identification of optimal hyperparameter settings, evaluation on the impacts of augmentation strategies, the use of differing fully connected layers and comparison of model accuracy when using existing model weights or retraining from scratch. As a result very high accuracies were achieved for the standalone CNN models. This subsequently led to creation of ensemble architecture models which attempted to refine classification accuracy further.

## REFERENCES

- [1] S. Łukasiewicz, M. Czelelewski, A. Forma, J. Baj, R. Sitarz, and A. Stanisławek, "Breast cancer—epidemiology, risk factors, classification, prognostic markers, and current treatment strategies—an updated review," *Cancers*, vol. 13, no. 17, p. 4287, 2021.
- [2] K. Fukushima, "Neocognitron: A self-organizing neural network model for a mechanism of pattern recognition unaffected by shift in position," *Biological cybernetics*, vol. 36, no. 4, pp. 193–202, 1980.
- [3] D. H. Hubel and T. N. Wiesel, "Receptive fields, binocular interaction and functional architecture in the cat's visual cortex," *The Journal of physiology*, vol. 160, no. 1, p. 106, 1962.
- [4] Y. LeCun, B. Boser, J. S. Denker, D. Henderson, R. E. Howard, W. Hubbard, and L. D. Jackel, "Backpropagation applied to handwritten zip code recognition," *Neural Computation*, vol. 1, no. 4, pp. 541–551, 1989.
- [5] Y. Lecun, L. Bottou, Y. Bengio, and P. Haffner, "Gradient-based learning applied to document recognition," *Proceedings of the IEEE*, vol. 86, no. 11, pp. 2278–2324, 1998.
- [6] O. Russakovsky, J. Deng, H. Su, J. Krause, S. Satheesh, S. Ma, Z. Huang, A. Karpathy, A. Khosla, M. Bernstein, A. C. Berg, and L. Fei-Fei, "ImageNet Large Scale Visual Recognition Challenge," *International Journal of Computer Vision (IJCV)*, vol. 115, no. 3, pp. 211–252, 2015.
- [7] A. Krizhevsky, I. Sutskever, and G. E. Hinton, "Imagenet classification with deep convolutional neural networks," *Advances in neural information processing systems*, vol. 25, 2012.
- [8] K. Simonyan and A. Zisserman, "Very deep convolutional networks for large-scale image recognition," *arXiv preprint arXiv:1409.1556*, 2014.
- [9] C. Szegedy, W. Liu, Y. Jia, P. Sermanet, S. Reed, D. Anguelov, D. Erhan, V. Vanhoucke, and A. Rabinovich, "Going deeper with convolutions," in *Proceedings of the IEEE conference on computer vision and pattern recognition*, 2014, pp. 1–9.
- [10] K. He, X. Zhang, S. Ren, and J. Sun, "Deep residual learning for image recognition," in *Proceedings of the IEEE conference on computer vision and pattern recognition*, 2016, pp. 770–778.
- [11] M. Tan and Q. Le, "Efficientnet: Rethinking model scaling for convolutional neural networks," in *International conference on machine learning*. PMLR, 2019, pp. 6105–6114.
- [12] G. Huang, Z. Liu, L. Van Der Maaten, and K. Q. Weinberger, "Densely connected convolutional networks," in *Proceedings of the IEEE conference on computer vision and pattern recognition*, 2017, pp. 4700–4708.
- [13] M. Sandler, A. Howard, M. Zhu, A. Zhmoginov, and L.-C. Chen, "Mobilenetv2: Inverted residuals and linear bottlenecks," in *Proceedings of the IEEE conference on computer vision and pattern recognition*, 2018, pp. 4510–4520.
- [14] B. Zoph, V. Vasudevan, J. Shlens, and Q. V. Le, "Learning transferable architectures for scalable image recognition," in *Proceedings of the IEEE conference on computer vision and pattern recognition*, 2018, pp. 8697–8710.
- [15] C. Carr, F. Kitamura, G. Partridge, inversion, J. Kalpathy-Cramer, J. Mongan, K. Andriole, Lavender, M. Vazirabad, M. Riopel, R. Ball, S. Dane, and Y. Chen, "Rsna screening mammography breast cancer detection," 2022.
- [16] G. Aresta, T. Araújo, S. Kwok, S. S. Chennamsetty, M. Safwan, V. Alex, B. Marami, M. Prastawa, M. Chan, M. Donovan *et al.*, "Bach: Grand challenge on breast cancer histology images," *Medical image analysis*, vol. 56, pp. 122–139, 2019.
- [17] International Agency for Research on Cancer - W.H.O. (2024) Press release no. 345. [Online]. Available:
- [18] F. Chollet, "Xception: Deep learning with depthwise separable convolutions," in *Proceedings of the IEEE conference on computer vision and pattern recognition*, 2017, pp. 1251–1258.
- [19] C. Szegedy, V. Vanhoucke, S. Ioffe, J. Shlens, and Z. Wojna, "Rethinking the inception architecture for computer vision," in *Proceedings of the IEEE conference on computer vision and pattern recognition*, 2016, pp. 2818–2826.
- [20] Z. Zhu, S.-H. Wang, and Y.-D. Zhang, "A survey of convolutional neural network in breast cancer," *Computer modeling in engineering & sciences: CMES*, vol. 136, no. 3, p. 2127, 2023.
- [21] F. A. Spanhol, L. S. Oliveira, C. Petitjean, and L. Heutte, "A dataset for breast cancer histopathological image classification," *Ieee transactions on biomedical engineering*, vol. 63, no. 7, pp. 1455–1462, 2015.
- [22] M. Gour, S. Jain, and T. Sunil Kumar, "Residual learning based cnn for breast cancer histopathological image classification," *International Journal of Imaging Systems and Technology*, vol. 30, no. 3, pp. 621–635, 2020.
- [23] F. A. Spanhol, L. S. Oliveira, C. Petitjean, and L. Heutte, "Breast cancer histopathological image classification using convolutional neural networks," in *2016 International Joint Conference on Neural Networks (IJCNN)*, 2016, pp. 2560–2567.
- [24] Y. Wang, L. Sun, K. Ma, and J. Fang, "Breast cancer microscope image classification based on cnn with image deformation," in *Image Analysis and Recognition: 15th International Conference, ICIAR 2018, Póvoa de Varzim, Portugal, June 27–29, 2018, Proceedings 15*. Springer, 2018, pp. 845–852.
- [25] K. Das, S. Conjeti, J. Chatterjee, and D. Sheet, "Detection of breast cancer from whole slide histopathological images using deep multiple instance cnn," *IEEE Access*, vol. 8, pp. 213 502–213 511, 2020.
- [26] M. Nawaz, A. A. Sewissy, and T. H. A. Soliman, "Multi-class breast cancer classification using deep learning convolutional neural network," *International Journal of Advanced Computer Science and Applications*, vol. 9, no. 6, 2018. [Online]. Available: <http://dx.doi.org/10.14569/IJACSA.2018.090645>
- [27] E. Deniz, A. Şengür, Z. Kadiroğlu, Y. Guo, V. Bajaj, and Ü. Budak, "Transfer learning based histopathologic image classification for breast cancer detection," *Health information science and systems*, vol. 6, pp. 1–7, 2018.
- [28] H. K. Mewada, A. V. Patel, M. Hassaballah, M. H. Alkinani, and K. Mahant, "Spectral-spatial features integrated convolution neural network for breast cancer classification," *Sensors*, vol. 20, no. 17, p. 4747, 2020.
- [29] A. Vidyarthi, J. Shad, S. Sharma, and P. Agarwal, "Classification of breast microscopic imaging using hybrid clahe-cnn deep architecture," in *2019 Twelfth International Conference on Contemporary Computing (IC3)*. IEEE, 2019, pp. 1–5.
- [30] N. Bayramoglu, J. Kannala, and J. Heikkilä, "Deep learning for magnification independent breast cancer histopathology image classification," in *2016 23rd International Conference on Pattern Recognition (ICPR)*, 2016, pp. 2440–2445.
- [31] A. Rakhlin, A. Shvets, V. Iglovikov, and A. A. Kalinin, "Deep convolutional neural networks for breast cancer histology image analysis," in *Image Analysis and Recognition: 15th International Conference, ICIAR 2018, Póvoa de Varzim, Portugal, June 27–29, 2018, Proceedings 15*. Springer, 2018, pp. 737–744.
- [32] M. Z. Alom, C. Yakopcic, M. S. Nasrin, T. M. Taha, and V. K. Asari, "Breast cancer classification from histopathological images with inception recurrent residual convolutional neural network," *Journal of digital imaging*, vol. 32, pp. 605–617, 2019.
- [33] A. Campilho, F. Karay, and B. ter Haar Romeny, "Preface: Image analysis and recognition: 15th international conference, icar 2018, póvoa de varzim, portugal, june 27-29, 2018, proceedings," *Lecture Notes in Computer Science*, vol. 10882, pp. 715–940, 2018.
- [34] C. Duggan, A. Dvaladze, A. F. Rositch, O. Ginsburg, C.-H. Yip, S. Horton, R. Camacho Rodriguez, A. Eniu, M. Mutebi, J.-M. Bourque *et al.*, "The breast health global initiative 2018 global summit on improving breast healthcare through resource-stratified phased implementation: methods and overview," *Cancer*, vol. 126, pp. 2339–2352, 2020.
- [35] N. Weiss, H. Kost, and A. Homeyer, "Towards interactive breast tumor classification using transfer learning," in *Image Analysis and Recognition: 15th International Conference, ICIAR 2018, Póvoa de Varzim, Portugal, June 27–29, 2018, Proceedings 15*. Springer, 2018, pp. 727–736.
- [36] C. Cortes and V. Vapnik, Support-vector networks. *Mach Learn* 20, 273–297. 1995. <https://doi.org/10.1007/BF00994018>
- [37] G. Ke, Q. Meng, T. Finley, T. Wang, W. Chen, W. Ma, Q. Ye and T. Y. Liu, 2017. Lightgbm: A highly efficient gradient boosting decision tree. *Advances in neural information processing systems*, 30
- [38] J. Friedman, T. Hastie and R. Tibshirani (2001). *The Elements of Statistical Learning*. Springer Series in Statistics Ch 10. DOI: 10.1007/b94608
- [39] L. Breiman. Random forests. *Machine learning*, 45, pp.5-32. 2001
- [40] A. H. A. Rahim, N. A. Rashid, A. Nayan, and A. Ahmad, "Smote approach to imbalanced dataset in logistic regression analysis," in *\*Proc. 3rd Int. Conf. Comput., Math., Statist. (iCMS2017) Transcending Boundaries, Embracing Multidisciplinary Diversities\**, Springer, 2019, pp. 429-433.
- [41] A. Ng, "CS229: Machine Learning - Support Vector Machines," Stanford University, 2020. [Online]. Available: <https://cs229.stanford.edu/notes2020spring/cs229-notes3.pdf>